Heliyon 6 (2020) e04274

Contents lists available at ScienceDirect

Heliyon

journal homepage: www.cell.com/heliyon

Research article

Impact of atmospheric boundary layer inhomogeneity in CFD simulations of tall buildings

Yousef Abu-Zidan *, Priyan Mendis, Tharaka Gunawardena

Department of Infrastructure Engineering, The University of Melbourne, VIC 3010, Australia

ARTICLE INFO

Keywords:
Civil engineering
Structural engineering
Computational fluid dynamics
Computer-aided engineering
Atmosphere modelling
Atmospheric boundary layer homogeneity
Tall building
CAARC
CFD simulation
Wind loading
Solution verification

ABSTRACT

Recently, there has been a growing interest in utilizing computational fluid dynamics (CFD) for wind analysis of tall buildings. A key factor that influences the accuracy of CFD simulations in urban environments is the homogeneity of the atmospheric boundary layer (ABL). This paper aims to investigate solution inaccuracies in CFD simulations of tall buildings that are due to ABL inhomogeneity. The investigation involves two steps. In the first step, homogenous and inhomogeneous ABL conditions are generated in an empty computational domain by employing two different modelling approaches. In the second step, the homogenous and inhomogeneous conditions are each applied to an isolated tall building, and simulation results are compared to investigate impact of ABL inhomogeneity on wind load predictions. The study finds that ABL inhomogeneity can be a significant source of error and may compromise reliability of wind load predictions. The largest magnitude of inhomogeneity error occurred for pressure predictions on the windward building surface. Shortening the upstream domain length reduced inhomogeneity errors but increased errors due to wind-blocking effects. The study proposes a practical approach for detecting ABL inhomogeneity that is based on monitoring sensitivity of key output metrics to variations in upstream domain length.

1. Introduction

Recently there has been a growing interest in utilising computational fluid dynamics (CFD) for wind design of tall buildings, and while CFD may offer considerable advantages such as reducing time and cost to solution and increasing design flexibility, it nonetheless presents a risk of degraded performance due to numerical errors and model uncertainties. Confidence in CFD predictions must be thoroughly established before this tool can be reliably adopted in the design of tall buildings.

The primary means for establishing confidence in computerized models that simulate physical reality is the verification and validation (V&V) framework (AIAA, 1998; Oberkampf and Trucano, 2002). This framework involves two consecutive steps. The first is verification, which assesses whether the numerical model has been correctly implemented in accordance with the modeller's conceptual description of the problem. This is followed by validation, where numerical results are compared with experiments to determine whether the numerical model can adequately replicate the physics of the problem. Verification is a vital prerequisite to validation and involves identifying and quantifying various sources of error in the simulation. The present study investigates one critical source of error in CFD simulations of tall buildings that is due to inhomogeneity of the atmospheric boundary layer (ABL).

ABL inhomogeneity refers to an unintended mismatch between the *inlet* and *incident* ABL profiles (see Figure 1), where wind conditions specified at the inlet boundary adapt as they travel through the computational domain to the location of the building. This issue typically manifests as an abrupt acceleration of flow near the ground surface, and a decline in velocity near the top of the domain (Blocken et al., 2007b; Hargreaves and Wright, 2007; Richards and Younis, 1990; Riddle et al., 2004). Maintaining a horizontally homogenous atmospheric boundary layer (HHABL) is imperative for solution reliability because it ensures that the wind conditions acting on the building are identical to those intended by the modeller. The importance of ABL homogeneity has been discussed in numerous computational wind engineering (CWE) studies for a wide range of applications including pedestrian wind comfort (Blocken et al., 2007a), building cross-ventilation (Ramponi and Blocken, 2012a, b), pollutant dispersion (Ai and Mak, 2013; Gorlé et al., 2009), wind-driven rain (Blocken and Carmeliet, 2006), flow around low rise buildings (Cindori et al., 2018; Gao and Chow, 2005; Longo et al., 2017; Parente et al., 2011; Yang et al., 2008), flow over complex terrains

* Corresponding author.
E-mail address: yabuzidan@gmail.com (Y. Abu-Zidan).

https://doi.org/10.1016/j.heliyon.2020.e04274
Received 19 April 2020; Received in revised form 25 May 2020; Accepted 18 June 2020

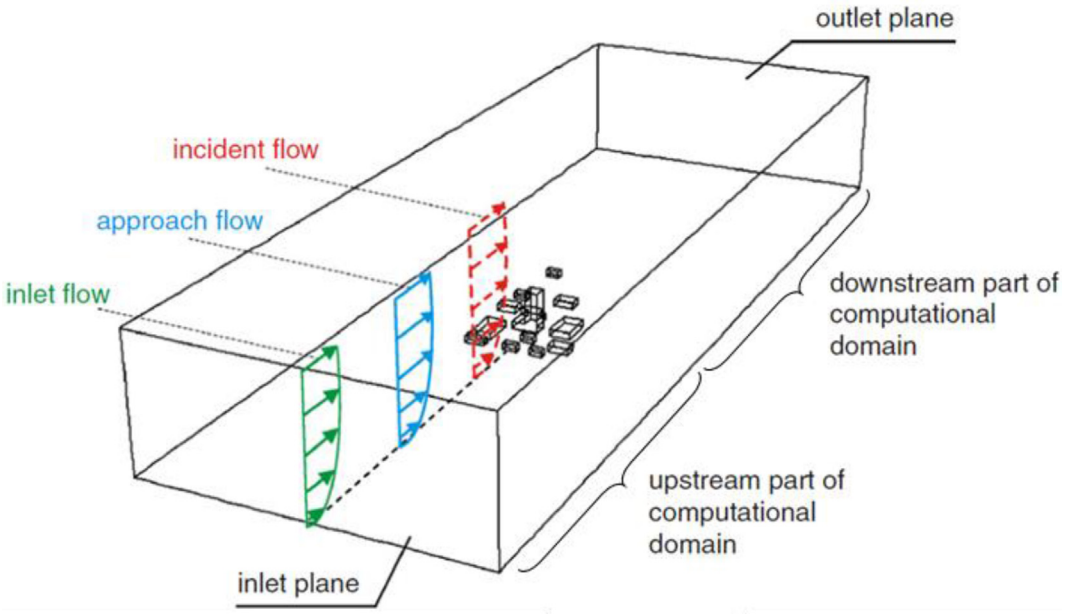

Figure 1. Inlet, incident, and approach ABL profiles in a CWE model (Blocken et al., 2007b).

(Balogh et al., 2012; Sørensen et al., 2007; Yan et al., 2016), and wind loading on tall buildings (Huang et al., 2007).

Dedicated studies on ABL inhomogeneity have largely focused on developing new modelling approaches with the aim of reducing ABL inhomogeneity while achieving realistic inflow conditions and accurate turbulence modelling [e.g. Balogh and Parente (2015); Balogh et al. (2012); Cindori et al. (2018); Gorlé et al. (2009); Juretić and Kozmar (2013); Longo et al. (2017); Parente et al. (2011); Pontiggia et al. (2009); Tian et al. (2014); Yan et al. (2016); Yang et al. (2009)]. Although these studies have made important advancements in reducing ABL inhomogeneity, to the authors' best knowledge, no study has comprehensively investigated and quantified the impact of ABL inhomogeneity on wind load predictions in tall buildings. Understanding the behaviour of inhomogeneity errors and its potential impact on wind load predictions will help establish confidence in CFD results for this application.

This paper investigates the impact of ABL inhomogeneity on CFD predictions of wind loads by considering the CAARC (Commonwealth Advisory Aeronautical Council) standard tall building. This paper comprises two complementary studies: (1) an investigation of ABL inhomogeneity in an empty domain, and (2) an investigation of the impact of ABL inhomogeneity on wind-induced surface pressures and base reactions for the CAARC tall building. In the first study, two distinct modelling approaches are employed to generate homogeneous and inhomogeneous ABL conditions in an empty domain, and the extent of ABL inhomogeneity is quantified by comparing incident and inlet profiles. In the second study, the CAARC tall building is exposed to each of the ABL conditions (homogenous and inhomogeneous) that were generated in the first step. Inhomogeneity errors are then quantified by comparing the resulting wind-induced pressures and base reactions under these two conditions.

Structurally, this paper is divided into 7 sections. First, Section 2 presents the theoretical background for achieving a HHABL in steady RANS. Section 3 describes the numerical setup of the simulations presented in this paper. Sections 4 and 5 present the results of the two studies in this paper. Finally, the results are discussed in Section 6 and the paper is concluded in Section 7.

2. Theoretical background

The requirements for a HHABL in RANS CFD simulations have been described in the early days of CWE by Richards and Hoxey (1993), who derived from theoretical principles the necessary boundary conditions that would achieve equilibrium with the standard turbulence kinetic energy (k)-(ε) dissipation rate of k turbulence model and prevent ABL inhomogeneity. These boundary conditions have made their way into numerous CWE guidelines (Blocken, 2015; Franke et al., 2007; Tominaga et al., 2008) and have become widely adopted by the CWE community. Despite this, the problem of ABL inhomogeneity persists in many CWE studies due to several reasons as mentioned below.

Hargreaves and Wright (2007) note that studies based on commercial CFD packages often implement only a subset of the requirements by Richards and Hoxey (1993). Specifically, the requirement of a driving shear force at the top of the domain is often ignored due to the technical difficulty in applying this condition, thereby resulting in ABL inhomogeneity. Blocken et al. (2007b) suggest that ABL inhomogeneity is largely caused by inherent limitations of the standard wall function in commercial CFD packages, such as FLUENT and CFX. These codes specify conflicting mesh requirements near the ground surface when modelling large-scale boundary layers, making it impossible to simultaneously satisfy ABL homogeneity conditions and numerical stability requirements of the solver. This issue was later resolved by Parente et al. (2011) for the k-ε model by developing a novel wall function based on aerodynamic roughness height aerodynamic terrain roughness height (z_0) instead of the equivalent sand-grain roughness equivalent sand-grain roughness (k_s) used in the standard wall function.

In many studies, however, ABL inhomogeneity simply occurs because the theoretical inlet profiles needed for homogeneity are disregarded in favour of experimental profiles that are more physically accurate but are incompatible with the turbulence model adopted in the simulation. To address this issue, numerous studies have proposed alternative ABL inlet profiles based on modified turbulence models [e.g. Balogh and Parente (2015); Balogh et al. (2012); Cindori et al. (2018); Gorlé et al. (2009); Juretić and Kozmar (2013); Longo et al. (2017); Parente et al. (2011);

Pontiggia et al. (2009); Tian et al. (2014); Yan et al. (2016); Yang et al. (2009)]. While these studies demonstrate the possibility of achieving homogenous profiles that more accurately reflect experimental conditions, they require the use of non-standard turbulence models that are not widely adopted in practice. Since validation with experimental results is beyond the scope of this paper, the current study will utilise standard RANS models for investigating issues of ABL inhomogeneity.

For RANS simulations, ABL homogeneity is achieved when the RANS equations are in balance with the turbulence model that approximates the turbulent nature of the flow in the computational domain, the wall function that describes the behaviour of the flow near the ground surface, and the inlet profile equations that characterise the flow entering the computational domain. Each of these conditions is discussed in detail below.

2.1. Turbulence model equations

The need for turbulence models arises from mathematical necessity to solve a closure problem in the Reynolds-averaged Navier-Stokes (RANS) equations. RANS equations are derived by applying the Reynolds averaging operator to the pure Navier-Stokes equations. According to this operator, each instantaneous flow variable can be conceived as the sum of a mean and a fluctuating component. The resulting RANS continuity and momentum equations are expressed in Cartesian tensor form as follow:

$$\frac{\partial \overline{u_i}}{\partial x_i} = 0 \tag{1}$$

$$\frac{\partial(\rho\overline{u_i})}{\partial t} + \frac{\partial\left(\rho\overline{u_i}\overline{u_j}\right)}{\partial x_j} = -\frac{\partial \overline{P}}{\partial x_i} + \frac{\partial}{\partial x_j}\left[\mu\left(\frac{\partial \overline{u_i}}{\partial x_j} + \frac{\partial \overline{u_j}}{\partial x_i}\right)\right] + \frac{\partial}{\partial x_j}\left(-\rho\overline{u_i'u_j'}\right) \tag{2}$$

The RANS equations are almost identical to the original Navier-Stokes equations but with time-averaged variables (denoted by a bar) replacing instantaneous variables. Notably, the RANS equations also include additional fluctuating terms that appear at the end of the momentum equation [Eq. (2)]. These are known as the Reynolds stress terms which account for the effect of turbulence on mean flow. In three-dimensional flow, the Reynolds stresses constitute six additional unknowns in the RANS equations, resulting in a closure problem where the number of unknowns is larger than the number of equations (Pope, 2000). Turbulence models provide additional relations which resolve the closure problem, allowing for a solution to be obtained.

In computational wind engineering applications, the two-equation k-ε turbulence models are widely adopted since they require significantly lower computational power than other non-linear RANS models. For the two-equation k-ε turbulence models, the Boussinesq approximation relates the Reynolds stresses $-\rho\overline{u_i'u_j'}$ to the mean flow strain rate as follows:

$$-\rho\overline{u_i'u_j'} = \mu_t\left(\frac{\partial u_i}{\partial x_j} + \frac{\partial u_j}{\partial x_i}\right) - \frac{2}{3}\rho k\delta_{ij} \tag{3}$$

where the turbulent (eddy) viscosity term dynamic eddy viscosity μ_t is a function of turbulence kinetic energy (k) and turbulence dissipation rate (ε):

$$\mu_t = C_\mu\rho\frac{k^2}{\varepsilon} \tag{4}$$

The Re-Normalisation Group (RNG) variant of the k-ε model (Yakhot et al., 1992) has been utilised in building studies due to its superior performance over the standard k-ε model which tends to overpredict the production of turbulence kinetic energy (Dagnew et al., 2009; Wright and Easom, 2003). The RNG variant of the k-ε model uses the following transport equations for k and ε:

$$\frac{\partial}{\partial x_i}(\rho k u_i) = \frac{\partial}{\partial x_j}\left(\alpha_k\mu_t\frac{\partial k}{\partial x_j}\right) + G_k - \rho\varepsilon \tag{5}$$

$$\frac{\partial}{\partial x_i}(\rho\varepsilon u_i) = \frac{\partial}{\partial x_j}\left(\alpha_\varepsilon\mu_t\frac{\partial \varepsilon}{\partial x_j}\right) + C_{1\varepsilon}\frac{\varepsilon}{k}G_k - C_{2\varepsilon}\rho\frac{\varepsilon^2}{k} \tag{6}$$

2.2. Near-wall treatment

Modelling of near-wall boundary layer flow in RANS is done using wall functions. These are semi-empirical descriptions of the boundary layer transition from the wall to the fully turbulent outer region of the flow. The most widely adopted of these is the standard wall function (SWF).

2.2.1. The standard wall function (SWF)

The SWF is derived based on the universal law-of-the-wall. In commercial CFD software FLUENT, the SWF is expressed as follows (ANSYS Inc., 2013):

$$\frac{Uu_*}{\tau_w/\rho} = \frac{1}{\kappa}\ln\left(E\frac{\rho u_* z}{\mu}\right) - \Delta B \tag{7}$$

For a fully rough flow regime, where the equivalent sand grain roughness dimensionless equivalent sand-grain roughness k_s^+ is ≥ 90 :

$$\Delta B = \frac{1}{\kappa}\ln\left(1 + C_s k_s^+\right) \tag{8}$$

For an equilibrium ABL where $u_* = u_\tau = \sqrt{\tau_w/\rho}$, Eq. (7) can be simplified as:

$$\frac{U}{u_*} = \frac{1}{\kappa}\ln\left(\frac{Ez^+}{1 + C_s k_s}\right) \approx \frac{1}{\kappa}\ln\left(\frac{Ez^+}{C_s k_s}\right) \tag{9}$$

The roughness parameter in the standard wall function is based on the equivalent sand-grain roughness height k_S. This is the predominant measure for roughness in industrial applications, and thus, is the default in most commercial CFD packages including FLUENT. For atmospheric flow, however, the aerodynamic roughness length z_0 is commonly used in lieu of k_s as a description of terrain roughness. The following equation relates the two measures of roughness in FLUENT (Blocken et al., 2007b):

$$k_s = \frac{Ez_0}{C_s} = \frac{9.793 z_0}{C_s} \tag{10}$$

While Eq. (10) has been adopted as standard CWE practice, its use is problematic in rough terrains with large z_0 values. This is due to conflicting sizing requirements of the wall-adjacent cells: to be sufficiently refined while having a centroid height centroid height of wall-adjacent element z_p greater than k_s (Blocken et al., 2007b). Additionally, the SWF does not calculate near-wall turbulence directly from roughness properties (Parente et al., 2011). As a result, achieving a HHABL is difficult with the standard wall function.

2.2.2. Modified wall function of Parente et al. (2011)

To overcome the inherent limitations of the SWF, Parente et al. (2011) derived an alternative near-wall function based on the aerodynamic roughness z_0 instead of the equivalent sand-grain roughness k_s. This modified wall function (MWF) is expressed as follows:

$$\frac{U}{u_*} = \frac{1}{\kappa}\ln\left(E' z^{+'}\right) \tag{11}$$

$$z^{+'} = \frac{(z + z_0)u_*}{\nu} \tag{12}$$

$$E' = \frac{\nu}{z_0 u_*} \tag{13}$$

The MWF [Eq. (11)] is mathematically analogous to the SWF [Eq. (9)], preserving the law-of-the-wall format. The main difference between the SWF and MWF is in the treatment of roughness. The MWF replaces the denominator $C_s k_s^+$ in the SWF with the modified wall function constant modified wall function constant E' as a function of z_0. This reformulation overcomes the limit on minimum height of wall-adjacent cells in the SWF. The MWF circumvents the requirement for $z_p > k_s$ by eliminating the need to define k_s altogether so that z_p can take any value. Additionally, the MWF ensures that the near-wall turbulence quantities are computed directly from the velocity function and its derivatives at the wall (Parente and Benocci, 2010).

Implementing the MWF in FLUENT is straightforward since FLUENT allows user-defined wall functions for k-ε RANS models. The user is required to specify expressions for the dimensionless velocity $U^* = U/u_*$, and its first and second derivatives with respect to the dimensionless distance from the wall $z^+ = zu_*/\nu$ (Monticelli, 2012). The following relations are hence derived from Eqs. (11), (12), and (13).

$$U^* = \frac{1}{\kappa}\ln\left(\frac{z^+\nu/u_* + z_0}{z_0}\right) \tag{14}$$

$$\frac{dU^*}{d(z^+)} = \frac{1}{\kappa}\left(\frac{\nu}{\nu z^+ + u_* z_0}\right) \tag{15}$$

$$\frac{d^2U^*}{d(z^+)^2} = -\frac{1}{\kappa}\left(\frac{\nu}{\nu z^+ + u_* z_0}\right)^2 \tag{16}$$

2.3. Inlet profile equations

The inlet conditions for a HHABL can be derived analytically by solving the turbulence model and wall function equations for equilibrium. Richards and Hoxey (1993) derived the following expressions for the standard k-ε model:

$$U = \frac{u_*}{\kappa}\ln\left(\frac{z + z_0}{z_0}\right) \tag{17}$$

$$k = \frac{u_*^2}{\sqrt{C_\mu}} \tag{18}$$

$$\varepsilon = \frac{u_*^3}{\kappa(z + z_0)} \tag{19}$$

with the constants $\kappa = 0.433$ and $C_\mu = 0.09$. Richards and Norris (2011) demonstrated that Eqs. (17), (18), and (19) are also valid for the RNG model with constants $\kappa = 0.4$ and $C_\mu = 0.085$.

3. Numerical setup

This section describes the numerical setup of the simulations performed in Sections 4 and 5 of this paper. This includes selection of inlet profiles, mesh configuration, domain size cases, and solver settings.

3.1. Selection of inlet profiles

An inlet velocity profile was selected based on Eq. (17), with ABL friction velocity $u_* = 1.12$ m/s and $z_0 = 2.0$ m. This profile corresponds to a reference velocity of reference mean wind speed at roof height $U_H = 12.7$ m/s at the top of the CAARC building (height of CAARC building $H = 182.9$ m, width of CAARC building $B = 45.7$ m, depth of building $D = 30.5$ m). The roughness length of $z_0 = 2.0$ m corresponds to a well-developed urban area where tall buildings are typically located (Wieringa, 1992). This high terrain roughness is ideal for the current study since it amplifies any potential issues with ABL inhomogeneity. Inlet profiles of k and ε are computed using Eqs. (18) and (19) respectively. It is worth noting that the expression in Eq. (18) results in a turbulence kinetic energy profile that is constant with height. While such a profile is not physically accurate in both wind tunnel tests and full-scale measurements (Huang et al., 2007; Juretić and Kozmar, 2013; Lim et al., 2016; Liu et al., 2003; Yang et al., 2009), it is still an acceptable and employable assumption for the purpose of assessing the limitations of horizontal inhomogeneities.

3.2. Mesh sensitivity analysis

A mesh sensitivity analysis is performed to ensure proper convergence of the solution with minimal spatial discretisation error. Three fully Cartesian mesh configurations of increasing refinement were generated with 0.75, 1.68, and 3.28 million elements. Figure 2 shows the refinement regions in the proximity of the building for the three mesh configurations.

The middle mesh configuration with 1.68 million elements was found to be sufficiently refined since it accurately reproduced results from the highly refined mesh of 3.28 million elements. Hence, the middle mesh was selected for the study, with a maximum element size of 1 m on the building surface, and a ground-adjacent cell height of 1.5 m ($z_p = 0.75$ m). A smoothly transitioning inflation layer from the building to the far-field was achieved with 10 layers of prismatic elements at an expansion ratio of 1.2.

3.3. Selection of domain size

The computational domain sizes selected for this study are presented in Table 1. These are based on best practice guidelines by Franke et al. (2007). The stream-wise length of the computational domain is divided into two portions: the upstream length spanning from the inlet boundary to the point of origin, and downstream length from the origin to the outlet (see Figure 3). The upstream length is varied between cases in order to assess the impact of travel distance on the horizontal homogeneity, while the downstream length is held constant for all cases in the study.

The origin in Figure 3 represents the location of incident profiles in the empty domain. It also represents the location of the tall building in the final model. As such, incident profiles characterise the unimpeded wind conditions that will be experienced by the building including any potential inhomogeneities. Under fully homogenous ABL conditions, incident profiles will coincide with inlet boundary profiles. For the sensitivity study performed in this paper, it was important to maintain a consistent mesh configuration between cases of different domain sizes, particularly in the immediate region surrounding the building. This is done to eliminate potential variation in the results that are due to variation in grid configuration between the cases being compared.

3.4. Solver settings

Simulations were performed in full geometric scale with a Reynolds number of 3.96×10^7 at the top of the building. CFD software FLUENT was selected as the RANS solver in this study. The RNG k-ε turbulence model was selected with $C_\mu = 0.085$. A pressure-based coupled solver (PBCS) was used with second order discretisation schemes for pressure and momentum terms. The solution was iterated until the scaled residual values dropped below 10^{-4}. This was deemed sufficient by monitoring the convergence of key output metrics in the model.

4. Assessing ABL homogeneity in an empty domain

The first study in this paper involves simulating ABLs in an empty domain in order to quantify the extent of ABL inhomogeneity in the incident profile. Two distinct modelling methods are used: *method A* which strictly adheres to the theoretical requirements for a HHABL (Parente et al., 2011; Richards and Hoxey, 1993; Richards and Norris,

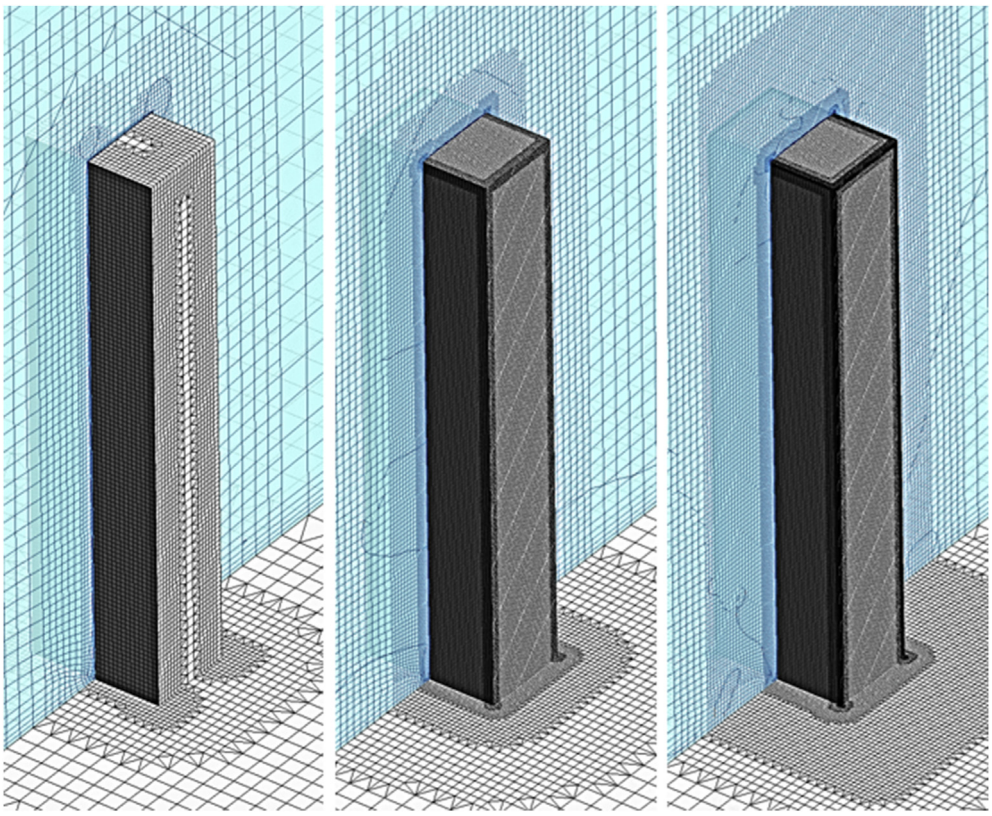

Figure 2. Mesh configurations with increasing element refinement in the proximity of the building (left to right: 0.75, 1.68, and 3.28 million elements).

Table 1. Summary of computational domain sizes used in this study.

Upstream length cases	Downstream length	Total domain width	Total domain height
3*H*	15*H**	2 × 5*H**	6*H**
5*H**			
10*H*			
15*H*			

* Recommended domain dimensions by Franke et al. (2007).

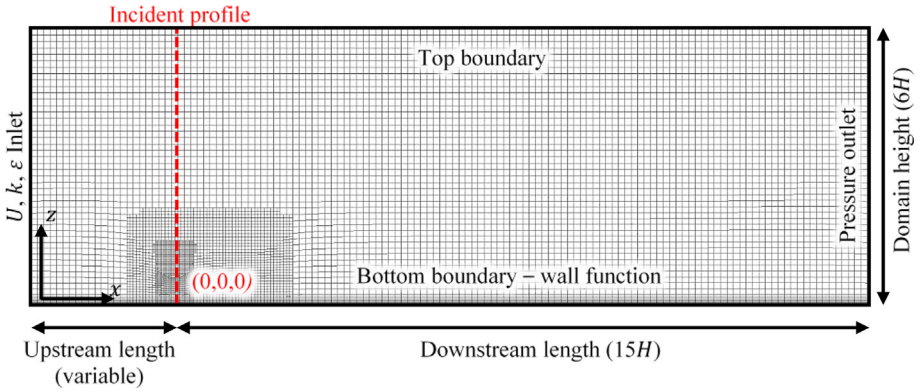

Figure 3. Empty computational domain showing mesh configuration and boundary conditions.

2011), and *method B* which reflects common practice in CWE studies. As the results of this study would later demonstrate, method A generates a homogenous ABL while method B produces inhomogeneous ABL conditions. The details of the two methods are outlined in Table 2.

The main difference between methods A and B are the boundary conditions at the top and bottom of the domain. Method A specifies a driving shear force $\tau = \rho u_*^2$ at the top boundary and adopts the MWF proposed by Parente et al. (2011) at the ground. On the other hand, method B neglects the top shear requirement and adopts the SWF at the ground surface where the equivalent sand-grain roughness is estimated with Eq. (10). The top shear requirement of method A is satisfied by implementing a stream-wise momentum source term at the topmost layer of elements in the domain. For both methods A and B, the upstream length is varied as specified in Table 1.

Table 2. Summary of simulation methods A and B used in this study.

	Method A	Method B
Inlet profiles	$U = \frac{u_*}{\kappa}\ln\left(\frac{z+z_0}{z_0}\right); k = \frac{u_*^2}{\sqrt{C_\mu}}; \varepsilon = \frac{u_*^3}{\kappa(z+z0)};$ $u_* = 1.12$ m/s; $z_0 = 2.0$ m; $C_\mu = 0.085$; $\kappa = 0.4$	
Outlet boundary condition	Static pressure outlet	
Top boundary condition	Driving shear stress: $\tau = \rho u_*^2$	Symmetry
Ground boundary condition	Modified wall function, based on aerodynamic length z_0 [Eqs. (11), (12), and (13)]	Standard wall function, FLUENT expression for equivalent sand-grain roughness k_S [Eq. (10)]
Side boundary condition	Symmetry	

4.1. Effect of modelling method on ABL homogeneity

ABL homogeneity is assessed in the empty domain by comparing incident profiles with inlet profiles. Figure 4 presents a graphical comparison of the velocity mean streamwise wind speed *(U)*, turbulence kinetic energy *(k)*, and turbulence dissipation rate *(ε)* incident and inlet profiles for the different upstream length cases. The plots on the left in Figure 4 are for simulations performed with method A, while the ones on the right are for method B. The plots begin at a height of $z = 2 \times z_p = 1.5$ m, since data points are located at the nodes of the Cartesian mesh.

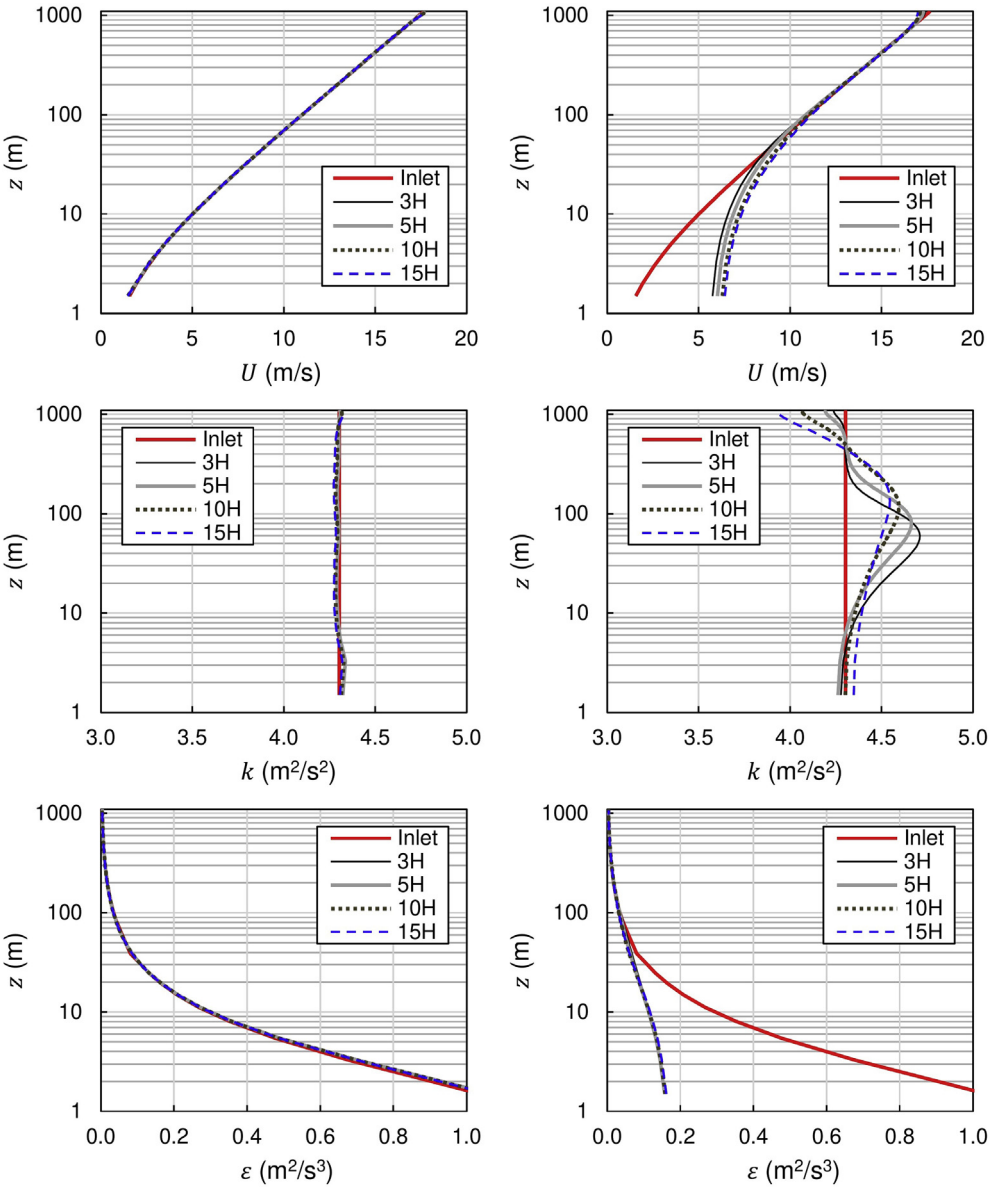

Figure 4. Inlet and incident U, k, and ε profiles simulated in an empty domain using method A (left) and method B (right). Vertical axes plotted in logarithmic scale.

As observed in Figure 4 (left), it is evident that method A is successful in maintaining a HHABL. The U, k, and ε incident profiles collapse onto the inlet profile for all upstream lengths. The combination of driving shear stress at the top boundary and the MWF at the ground was effective to preserve flow conditions throughout the entirety of the domain.

Conversely, the incident profiles in Figure 4 (right) deviate significantly from inlet conditions, particularly near the ground surface. The incident velocity near the ground accelerates by up to threefold, but this deviation decreases with height away from the ground. The incident k profiles also show a noticeable deviation from the constant k profile specified at the inlet, both at the top of the domain and at moderate heights. The large deviations in Figure 4 (right) demonstrate that method B fails to preserve inlet ABL profiles throughout the computational domain. Hence, method B can be said to cause ABL inhomogeneity.

The lack of driving shear stress at the top boundary in method B resulted in a reduction of both the velocity (by $< 4\%$) and turbulence kinetic energy (by 5.5–8.7%) quantities at that location. The reduction in k is larger than the reduction in velocity, particularly for longer upstream lengths. Moreover, the reduction of k propagates downwards more rapidly and contributes to the total deviation of turbulence kinetic energy in the vicinity of the building (5.7–9.5%). This is a potential source of error when predicting wind-induced forces on the building. Hence, a driving shear stress condition is recommended even if reduction in velocity profile at the top of the domain seems minimal.

4.2. Effect of upstream length

In Figure 5, the percentage velocity error for method B is plotted as a function of travel distance at multiple heights. Near the ground ($z = 10$ m and $z = 30$ m), Figure 5 shows a sudden adaptation as the profile enters the computational domain, eventually levelling off at large error values (50% and 15%, respectively). This abrupt adaptation of velocity near the ground signifies the failure of the SWF in replicating the high-roughness conditions of the inlet profile.

Moreover, this abrupt adaptation entails that the commonly used remedial measure for controlling ABL inhomogeneity by means of shortening the upstream domain length may be unviable for highly rough terrains. To illustrate this point, consider that limiting velocity deviations in Figure 5 to within $\pm$ 5% at $z = 10$ m requires an upstream length no longer than 83.9 m which is considerably shorter than the recommended minimum of 5H (930 m) by Franke et al. (2007).

Short upstream lengths can introduce errors due to the wind-blocking effect. The term "wind-blocking effect" refers to disturbances in the wind flow pattern caused by the presence of the building which is characterized by a slowing down of wind speed in front of the building and a build-up of pressure that causes flow to deflect over and around the building (Blocken and Carmeliet, 2006). For domains with very short upstream lengths, the inlet boundary may fall within the wind-blocking region that forms in front of the building. This would cause inlet velocity profiles to be imposed at a location where, realistically, the flow ought to slow down. In turn, this results in overprediction of positive pressures on windward building surfaces and overprediction of negative pressures on leeward, sides, and top surfaces (Abu-Zidan, 2019). Errors in wind load predictions due to this effect will be referred to as "wind-blocking errors" in this study.

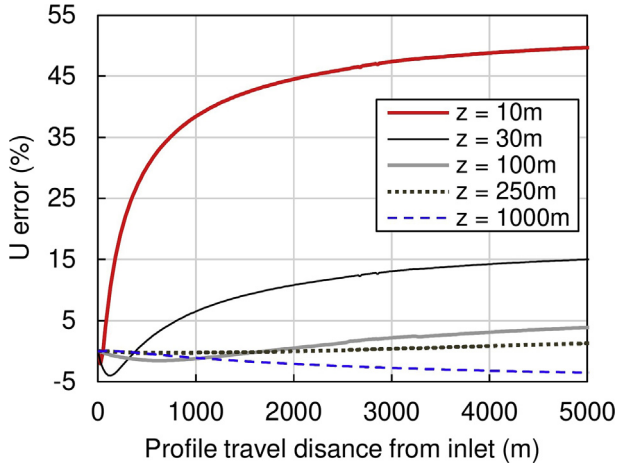

Figure 5. Percentage difference of U from inlet conditions as a function of travel distance at multiple heights. Simulation performed in empty domain with total length of 30H (upstream length = 15H, downstream length = 15H).

The term "wind-blocking effect" should not be confused with "blockage effects" that occurs in wind tunnels and CWE models. Blockage effects refer to the contraction of flow cross-sectional area due to the presence of a building model that causes an increase in flow velocity around the model. In this study, errors due to blockage effects are minimised by providing sufficient lateral and vertical domain dimensions to achieve a very low blockage ratio of (0.4%). This is the ratio of the projected frontal area of the building to the total cross-sectional area of the domain. Moreover, the blockage ratio is held constant to ensure blockage effects are equivalent for all simulation cases in the study.

5. Impact of ABL inhomogeneity on wind-induced building loads

In the previous section, the impact of ABL inhomogeneity on incident profiles was investigated and a method for achieving fully homogeneous conditions was demonstrated in an empty computational domain. In this section, a second study is performed to assess the impact of ABL inhomogeneity on wind load predictions on the CAARC tall building. To perform this investigation, the building is introduced to the empty domain at the location of the origin in Figure 3. Then, the building is exposed to the same homogenous and inhomogeneous conditions from Section 4 by implementing methods A and B, respectively. As in Section 4, the upstream length of the computational domain is varied in accordance with Table 1. All other parameters are kept identical to Section 4, including boundary conditions, ground wall functions, turbulence model, solution scheme, and mesh configuration (except at the immediate location where the building is introduced). This ensures that the wind loads presented in this section directly correspond to the incident profiles reported in Section 4. The building has full-scale dimensions of $B = 45.7$ m (width), $D = 30.5$ m (depth), and $H = 182.9$ m (height). A smooth SWF ($k_s = 0$) is specified on all surfaces of the building.

For wind load variables presented in this section, ABL inhomogeneity errors are simply the deviation of results under inhomogeneous conditions from results under homogenous conditions. The homogeneous case (method A) with the largest upstream distance (15H) is selected as the base case (BC) in this study. Deviations from the base case are considered errors.

5.1. Impact on wind-induced building pressure

Figure 6 presents wind-induced surface pressure coefficient C_P profiles at the centreline of the windward and leeward surfaces of the CAARC building under HHABL conditions. The various plots correspond to different upstream domain lengths as per Table 1. Figure 7 presents similar profiles under inhomogeneous conditions. Here, only the profiles along the building's centreline are presented as this is where critical pressure values and maximum inhomogeneity errors typically occur.

It can be seen in Figure 6 that the homogenous ABL conditions from method A resulted in identical C_P profiles for all upstream lengths (aside from 3H) with minimal deviations of $<$2.1% from the base case. This was expected since method A has already been shown to produce incident profiles that do not vary with upstream domain length (Figure 4, left). The C_P profiles for the 5H, 10H, and 15H cases represent almost perfect homogenous conditions as evidenced by their insensitivity to upstream domain length. Interestingly, the 3H case in Figure 6 showed some

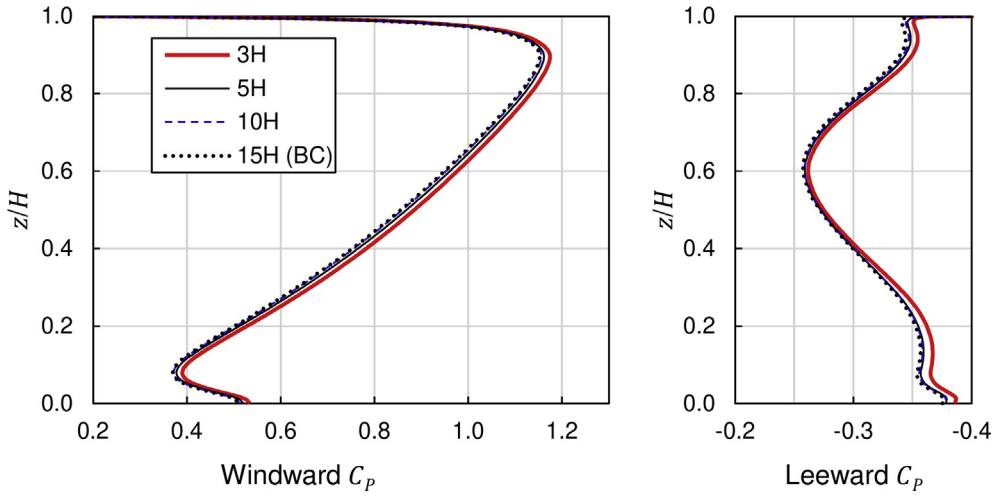

Figure 6. Windward and leeward pressure coefficient distributions along the centreline of the building under homogenous ABL conditions (method A). BC = Base case. C_P normalised with reference velocity = U_H.

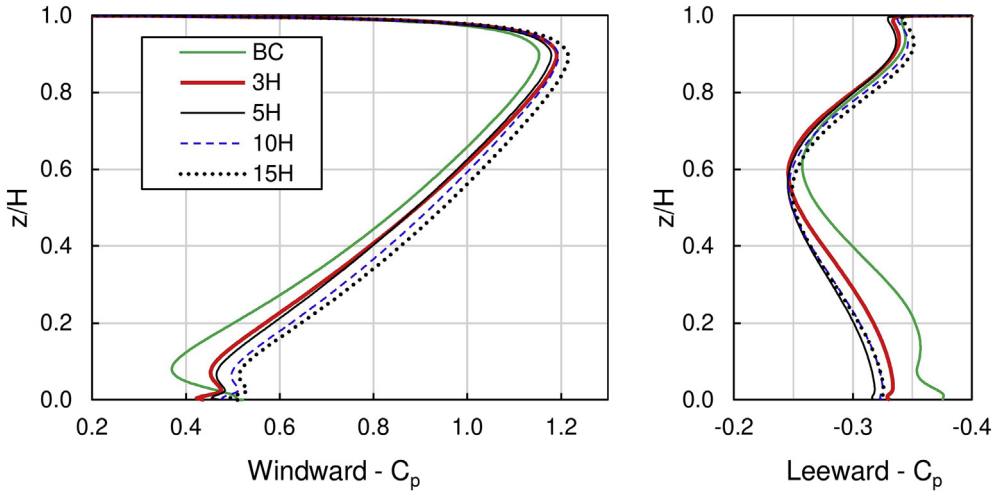

Figure 7. Windward and leeward pressure coefficient distributions along the centreline of the building under inhomogeneous ABL conditions (method B). BC = Base case of 15H upstream length and homogenous conditions (method A).

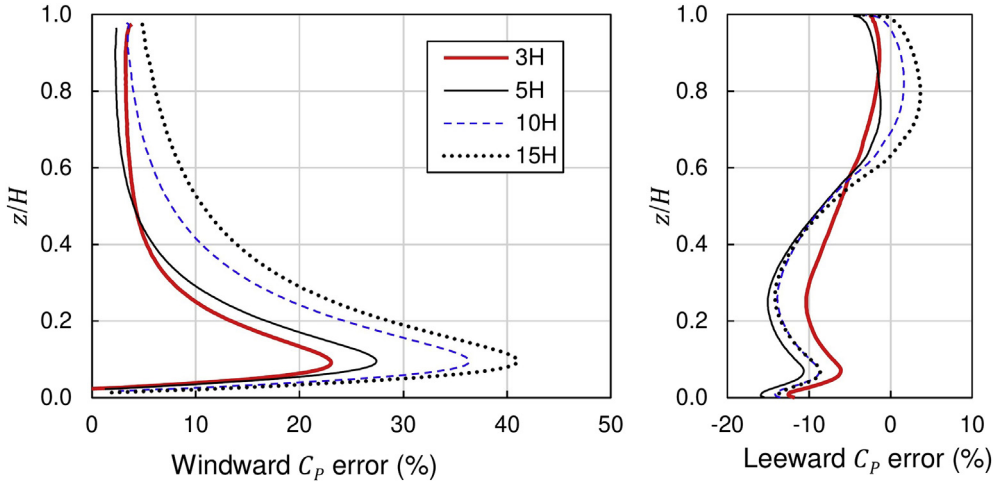

Figure 8. Percentage error in pressure coefficient along the centreline of windward (left) and leeward (right) surfaces under inhomogeneous ABL conditions (method B).

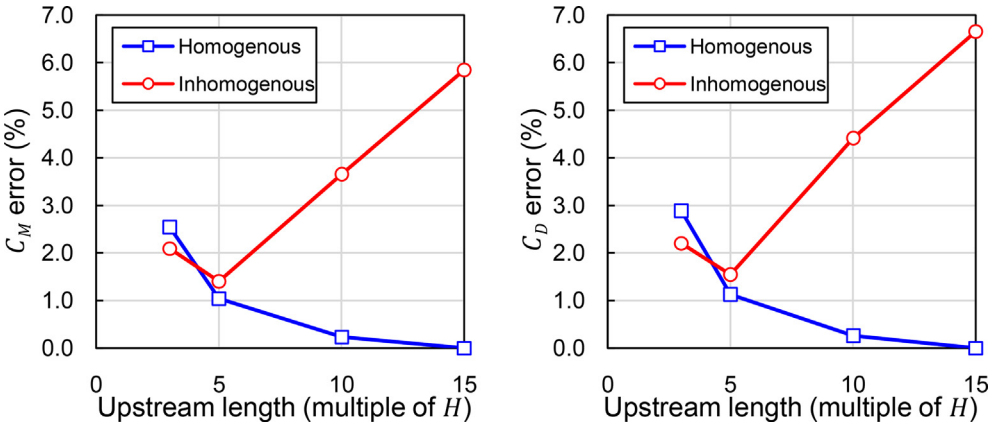

Figure 9. Percentage error in along-wind building base moment (left) and shear (right) for different upstream lengths and ABL homogeneity conditions. Base case C_M = 0.575 and C_D = 1.254 normalised with reference velocity = U_H, width = B, and height = H.

deviation in both the windward and leeward C_P plots (maximum of 5.6%). Nevertheless, these deviations cannot be attributed to inhomogeneity errors since no such behaviour occurs in the corresponding incident profiles (Figure 4, left). Instead, this behaviour is likely due to wind-blocking effects caused by a short upstream domain length.

In contrast to Figure 6, it can be seen in Figure 7 that the inhomogeneous ABL conditions from method B produced C_P plots that are highly sensitive to upstream domain length. Once again, this behaviour is expected since method B has already been shown to produce incident profiles that vary significantly with upstream domain length (Figure 4, right). All the C_P plots in Figure 7 deviated considerably from the homogenous base case (plotted in green). The percentage error in the C_P profiles are plotted in Figure 8 to further investigate the nature of inhomogeneity errors on pressure predictions.

It can be seen in Figure 8 that inhomogeneity errors in C_P occur at all heights of the building, but they are largest near the bottom region of both windward and leeward surfaces. For the windward surface, C_P errors increase significantly with upstream length. The volatile nature of these errors is clearly demonstrated in Figure 8 (left), which signifies the large degree of uncertainty in the solution. Similarly, leeward C_P errors are noticeable (Figure 8, right), albeit lower in magnitude compared to windward errors. The relationship between leeward C_P errors and upstream length is not immediately obvious.

When comparing inhomogeneity trends in the incident velocity profile (Figure 4, U plot, right) with errors in windward C_P (Figure 8, left), the two plots exhibit similar behaviour. The maximum error for both occurs near the bottom, and both errors increase with upstream length. While such similarity is expected since windward pressure is largely dictated by the approach wind speed, the correlation between the two is not exact. For instance, the deviation in incident velocity at the ground surface reaches values of up to 300%, whereas windward C_P error at the ground is close to zero. This suggests that wind-induced loading may be influenced by multiple factors aside from wind speed such as the building geometry and the turbulence kinetic energy profile. Therefore, pressure inhomogeneity errors cannot be reliably predicted from variations in the incident velocity profile.

5.2. Impact on base moment and shear

The along-wind base moment coefficients (C_M) and building base shear (C_D) are key design metrics for tall buildings since they represent the overall lateral wind loading on the structure. The impact of ABL inhomogeneity errors on base moment and shear is assessed by computing the percentage deviation of these metrics from the base case. The results of this analysis are presented in Figure 9.

Figure 9 shows that the behaviour of error in base moment C_M and base shear C_D are identical. To explain the trends seen in Figure 9, consider the two main sources of error in the simulation, both of which cause an overprediction of windward pressure. The first error is due to ABL inhomogeneity which increases with upstream domain length. The second is due to wind-blocking effects in short domains, which decreases with upstream domain length. So, as the upstream length of the domain is increased, wind-blocking errors disappear while inhomogeneity errors become dominant.

Initially, the decrease in wind-blocking error between cases 3H to 5H in Figure 9 is greater than the increase in inhomogeneity error. As a result, the total error drops between 3H and 5H for both homogenous (blue lines) and inhomogeneous cases (red lines). Between 5H and 15H, the total error for the homogenous case (blue line) continues to decrease with upstream length. This is because wind-blocking error continues to decrease with upstream length while inhomogeneity error is absent. For the inhomogeneous cases (red lines), the total error increases considerably between 5H and 15H as inhomogeneity error becomes dominant.

The maximum error in C_M and C_F is significantly less than the maximum error in windward C_P. For instance, the error in C_M and C_D for the 15H case is 6–7% (Figure 9), whereas the maximum error in windward C_P for the same case is 40% (Figure 8 left). This indicates that wind-induced base reactions are not strongly influenced by highly erroneous, yet localised, C_P values. The magnitude of base reaction error is therefore not a reliable indicator for the overall accuracy of the solution. Nonetheless, monitoring base reaction error can be effective for detecting wind-blocking effects due to short upstream domain lengths.

6. Discussion of results

For the high-roughness ABL used in this study, the commonly adopted modelling method B resulted in large inhomogeneity errors that significantly impacted the accuracy of predicted wind loading on the tall building. These errors were particularly large in pressure values on the windward surface of the building, reaching up to 40%. The errors also appear in the base reactions of the building but with a smaller maximum magnitude of 6–7%. Due to the potentially large value of these errors, tall building simulations must always be verified against inhomogeneity errors prior to validation with experimental data.

While CWE guidelines recommend testing for ABL inhomogeneity errors, many tall building studies do not report these assessments, and address the issue by mentioning the use of some remedial measure, such as shortening the upstream length of the computational domain. The results of this study show that these remedial measures do not always guarantee the containment of inhomogeneity errors and can introduce other sources of error such as wind-blocking effects in domains with very short upstream lengths. Hence, regardless of whether remedial measures are adopted, it is still vital to test and report inhomogeneity errors in order to establish confidence in the solution.

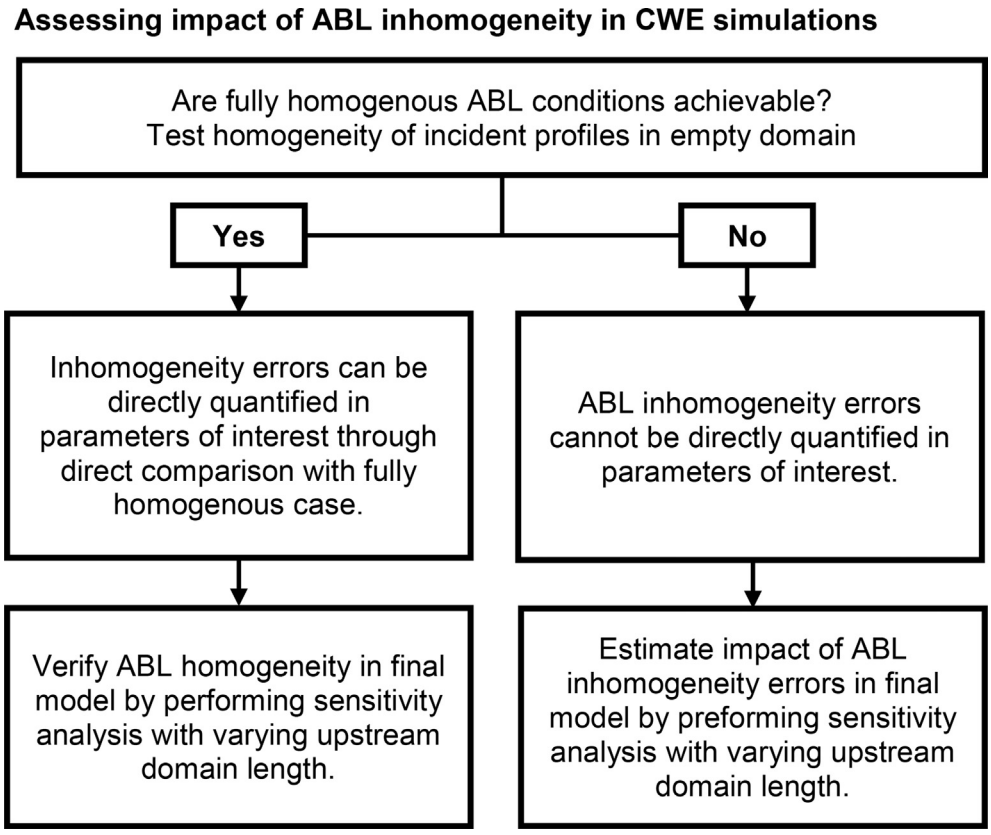

Figure 10. Framework for assessing impact of ABL inhomogeneity errors in CWE simulations.

The recommended method for ABL homogeneity assessment in CWE guidelines is to perform simulations in an empty domain and report the incident profiles to which the final model would be subjected (Blocken, 2015; Franke et al., 2007; Tominaga et al., 2008). The main drawback with this approach is that it does not evaluate errors in the output variables of the final model. Hence, a more effective approach for assessing the impact of ABL inhomogeneity is hereby proposed and outlined in Figure 10:

- The first step is to attempt to achieve an HHABL by meeting the theoretical requirements for homogeneity. This exercise is best performed in an empty domain where ABL inhomogeneity can be directly evaluated from the incident profiles. This assessment should not be limited to velocity profiles since variations in other flow quantities, such as k, can have a significant impact on wind-induced loading on the building.
- If an HHABL is achievable, the next step is to assess inhomogeneity errors in the final model. This is done with a sensitivity analysis by varying the upstream length of the domain and monitoring key design metrics. For wind loading on tall buildings, these parameters include surface pressures and building base reactions. Aside from cases with very short upstream lengths that would introduce wind-blocking errors, the output variables should remain unchanged when varying upstream domain length if inhomogeneity errors are indeed absent.
- If an HHABL cannot be achieved, then the exact magnitude of ABL inhomogeneity errors cannot be directly quantified. In this case, an approximate assessment of ABL inhomogeneity errors can be performed by quantifying variation in output parameters with changes in the upstream domain length. These variations will exhibit similar trends to those in the actual error plots, despite having lower magnitudes. While the value of inhomogeneity errors cannot be exactly determined, this approach is effective in identifying cases where ABL inhomogeneity errors are unacceptably large.

7. Conclusions

This study presents an investigation into ABL inhomogeneity error and its impact on CFD simulations of a tall building. The following findings of this investigation are noteworthy:

- ABL inhomogeneity can be a significant source of error in wind loading simulations of tall buildings. Detecting this error is therefore an essential verification activity that is needed in order to establish confidence in the numerical solution.
- ABL inhomogeneity in steady RANS is primarily due to the failure of the standard wall function in reproducing high-roughness terrain conditions, despite adopting the recommended roughness expression from CWE guidelines. A fully HHABL can be achieved for the RNG k-ε model using a modified wall function at the ground, and a driving shear stress at the top of the domain.
- ABL inhomogeneity errors in this study were particularly dominant in pressure values on the windward surface of the building. This error increased for larger upstream domain lengths.
- For very short upstream domain lengths, errors due to ABL inhomogeneity subsided, while errors due to wind-blocking effects became significant. Monitoring errors in base reaction values is effective for detecting blockage effects due to very short upstream domain lengths.
- ABL inhomogeneity can be practically assessed by evaluating the sensitivity of key output metrics to variations in upstream domain length. Under perfectly homogenous ABL conditions, the output metrics should not vary with upstream domain length except for very short domains where wind-blocking effects are likely to occur.

The findings of this study provide valuable insight into the behaviour of ABL inhomogeneity errors and help inform verification activities relating to this error. However, the study has limitations that must be

mentioned. Most notably, the study was performed using steady RANS models and these are not capable of simulating dynamic wind effects such as vortex shedding which often governs tall building design. Such effects can be simulated using scale resolving simulations, such as Large Eddy Simulations (LES), but these have a much greater computational cost compared to RANS. Nonetheless, for the purposes of investigating the adverse effects of ABL inhomogeneities, the RANS models used in this study are deemed satisfactory. Many of the findings and recommendations of the present study are valid for cases where hybrid RANS/LES simulations are used; although further research is needed to more comprehensively extend these findings to unsteady simulations.

Declarations

Author contribution statement

Yousef Abu-Zidan: Conceived and designed the experiments; Performed the experiments; Analyzed and interpreted the data; Wrote the paper.

Priyan Mendis & Tharaka Gunawardena: Conceived and designed the experiments; Wrote the paper.

Funding statement

The research was supported by an Australian Government Research Training Program (RTP) Scholarship, and the Australian Research Council Industrial Transformation Research Programme IC150100023: ARC Training Centre for Advanced Manufacturing of Prefabricated Housing.

Competing interest statement

The authors declare no conflict of interest.

Additional information

No additional information is available for this paper.

References

Abu-Zidan, Y.F., 2019. Verification and Validation Framework for Computational Fluid Dynamics Simulation of Wind Loads on Tall Buildings. Department of Infrastructure Engineering. The University of Melbourne.

Ai, Z.T., Mak, C.M., 2013. CFD simulation of flow and dispersion around an isolated building: effect of inhomogeneous ABL and near-wall treatment. Atmos. Environ. 77, 568–578.

AIAA, 1998. Guide for the Verification and Validation of Computational Fluid Dynamics Simulations (AIAA G-077-1998(2002)). American Institute of Aeronautics and Astronautics, Inc.

ANSYS Inc, 2013. ANSYS Fluent Theory Guide, USA.

Balogh, M., Parente, A., 2015. Realistic boundary conditions for the simulation of atmospheric boundary layer flows using an improved k–ε model. J. Wind Eng. Ind. Aerod. 144, 183–190.

Balogh, M., Parente, A., Benocci, C., 2012. RANS simulation of ABL flow over complex terrains applying an Enhanced k-ε model and wall function formulation: implementation and comparison for fluent and OpenFOAM. J. Wind Eng. Ind. Aerod. 104–106, 360–368.

Blocken, B., 2015. Computational Fluid Dynamics for urban physics: importance, scales, possibilities, limitations and ten tips and tricks towards accurate and reliable simulations. Build. Environ. 91, 219–245.

Blocken, B., Carmeliet, J., 2006. The influence of the wind-blocking effect by a building on its wind-driven rain exposure. J. Wind Eng. Ind. Aerod. 94, 101–127.

Blocken, B., Carmeliet, J., Stathopoulos, T., 2007a. CFD evaluation of wind speed conditions in passages between parallel buildings—effect of wall-function roughness modifications for the atmospheric boundary layer flow. J. Wind Eng. Ind. Aerod. 95, 941–962.

Blocken, B., Stathopoulos, T., Carmeliet, J., 2007b. CFD simulation of the atmospheric boundary layer: wall function problems. Atmos. Environ. 41, 238–252.

Cindori, M., Juretić, F., Kozmar, H., Džijan, I., 2018. Steady RANS model of the homogeneous atmospheric boundary layer. J. Wind Eng. Ind. Aerod. 173, 289–301.

Dagnew, A.K., Bitsuamalk, G.T., Merrick, R., 2009. Computational evaluation of wind pressures on tall buildings. In: Proceedings of the 11th Americas Conference on Wind Engineering.

Franke, J., Hellsten, A., Schlünzen, H., Carissimo, B., 2007. Best Practice Guideline for the CFD Simulation of Flows in the Urban Environment. COST Office, Brussels.

Gao, Y., Chow, W.K., 2005. Numerical studies on air flow around a cube. J. Wind Eng. Ind. Aerod. 93, 115–135.

Gorlé, C., van Beeck, J., Rambaud, P., Van Tendeloo, G., 2009. CFD modelling of small particle dispersion: the influence of the turbulence kinetic energy in the atmospheric boundary layer. Atmos. Environ. 43, 673–681.

Hargreaves, D.M., Wright, N.G., 2007. On the use of the k– model in commercial CFD software to model the neutral atmospheric boundary layer. J. Wind Eng. Ind. Aerod. 95, 355–369.

Huang, S., Li, Q.S., Xu, S., 2007. Numerical evaluation of wind effects on a tall steel building by CFD. J. Constr. Steel Res. 63, 612–627.

Juretić, F., Kozmar, H., 2013. Computational modeling of the neutrally stratified atmospheric boundary layer flow using the standard k–ε turbulence model. J. Wind Eng. Ind. Aerod. 115, 112–120.

Lim, K.E.W., Watkins, S., Clothier, R., Ladani, R., Mohamed, A., Palmer, J.L., 2016. Full-scale flow measurement on a tall building with a continuous-wave Doppler Lidar anemometer. J. Wind Eng. Ind. Aerod. 154, 69–75.

Liu, G., Xuan, J., Park, S.-U., 2003. A new method to calculate wind profile parameters of the wind tunnel boundary layer. J. Wind Eng. Ind. Aerod. 91, 1155–1162.

Longo, R., Ferrarotti, M., Sánchez, C.G., Derudi, M., Parente, A., 2017. Advanced turbulence models and boundary conditions for flows around different configurations of ground-mounted buildings. J. Wind Eng. Ind. Aerod. 167, 160–182.

Monticelli, M., 2012. Generalized wall Functions for RANS Computation of Turbulent Flows. Department of Energy. Polytechnic University of Milan.

Oberkampf, W.L., Trucano, T.G., 2002. Verification and validation in computational fluid dynamics. Prog. Aero. Sci. 38, 209–272.

Parente, A., Benocci, C., 2010. On the RANS simulation of neutral ABL flows. In: Proceedings of the Fifth International Symposium on Computational Wind Engineering (CWE2010).

Parente, A., Gorlé, C., van Beeck, J., Benocci, C., 2011. Improved k–ε model and wall function formulation for the RANS simulation of ABL flows. J. Wind Eng. Ind. Aerod. 99, 267–278.

Pontiggia, M., Derudi, M., Busini, V., Rota, R., 2009. Hazardous gas dispersion: a CFD model accounting for atmospheric stability classes. J. Hazard Mater. 171, 739–747.

Pope, S.B., 2000. Turbulent Flows. Cambridge University Press.

Ramponi, R., Blocken, B., 2012a. CFD simulation of cross-ventilation flow for different isolated building configurations: validation with wind tunnel measurements and analysis of physical and numerical diffusion effects. J. Wind Eng. Ind. Aerod. 104–106, 408–418.

Ramponi, R., Blocken, B., 2012b. CFD simulation of cross-ventilation for a generic isolated building: impact of computational parameters. Build. Environ. 53, 34–48.

Richards, P.J., Hoxey, R.P., 1993. Appropriate boundary conditions for computational wind engineering models using the k-ε turbulence model. J. Wind Eng. Ind. Aerod. 46–47, 145–153.

Richards, P.J., Norris, S.E., 2011. Appropriate boundary conditions for computational wind engineering models revisited. J. Wind Eng. Ind. Aerod. 99, 257–266.

Richards, P.J., Younis, B.A., 1990. Comments on "prediction of the wind-generated pressure distribution around buildings" by E.H. Mathews. J. Wind Eng. Ind. Aerod. 34, 107–110.

Riddle, A., Carruthers, D., Sharpe, A., McHugh, C., Stocker, J., 2004. Comparisons between FLUENT and ADMS for atmospheric dispersion modelling. Atmos. Environ. 38, 1029–1038.

Sørensen, N.N., Bechmann, A., Johansen, J., Myllerup, L., Botha, P., Vinther, S., Nielsen, B.S., 2007. Identification of severe wind conditions using a Reynolds Averaged Navier-Stokes solver. J. Phys. Conf. 75, 012053.

Tian, L.L., Zhu, W.J., Shen, W.Z., Sørensen, J.N., Zhao, N., 2014. Investigation of modified AD/RANS models for wind turbine wake predictions in large wind farm. J. Phys. Conf. 524, 012151.

Tominaga, Y., Mochida, A., Yoshie, R., Kataoka, H., Nozu, T., Yoshikawa, M., Shirasawa, T., 2008. AIJ guidelines for practical applications of CFD to pedestrian wind environment around buildings. J. Wind Eng. Ind. Aerod. 96, 1749–1761.

Wieringa, J., 1992. Updating the Davenport roughness classification. J. Wind Eng. Ind. Aerod. 41, 357–368.

Wright, N.G., Easom, G.J., 2003. Non-linear k–ε turbulence model results for flow over a building at full-scale. Appl. Math. Model. 27, 1013–1033.

Yakhot, V., Orszag, S.A., Thangam, S., Gatski, T.B., Speziale, C.G., 1992. Development of turbulence models for shear flows by a double expansion technique. Phys. Fluids 4, 1510–1520.

Yan, B.W., Li, Q.S., He, Y.C., Chan, P.W., 2016. RANS simulation of neutral atmospheric boundary layer flows over complex terrain by proper imposition of boundary conditions and modification on the k-ε model. Environ. Fluid Mech. 16, 1–23.

Yang, W., Quan, Y., Jin, X., Tamura, Y., Gu, M., 2008. Influences of equilibrium atmosphere boundary layer and turbulence parameter on wind loads of low-rise buildings. J. Wind Eng. Ind. Aerod. 96, 2080–2092.

Yang, Y., Gu, M., Chen, S., Jin, X., 2009. New inflow boundary conditions for modelling the neutral equilibrium atmospheric boundary layer in computational wind engineering. J. Wind Eng. Ind. Aerod. 97, 88–95.